HHS Public Access

Author manuscript

Sci Signal. Author manuscript; available in PMC 2017 May 03.

Published in final edited form as:

Sci Signal. ; 10(460): . doi:10.1126/scisignal.aah4117.

The SCF$^{\beta\text{-TRCP}}$ E3 ubiquitin ligase complex targets Lipin1 for ubiquitination and degradation to promote hepatic lipogenesis

Kouhei Shimizu[1,2,†], **Hidefumi Fukushima**[2,†], **Kohei Ogura**[1,3], **Evan C. Lien**[1], **Naoe Taira Nihira**[1], **Jinfang Zhang**[1], **Brian J. North**[1], **Ailan Guo**[4], **Katsuyuki Nagashima**[5], **Tadashi Nakagawa**[6], **Seria Hoshikawa**[2,7], **Asami Watahiki**[2], **Koji Okabe**[5], **Aya Yamada**[7], **Alex Toker**[1], **John M. Asara**[8], **Satoshi Fukumoto**[2,7], **Keiichi I. Nakayama**[9], **Keiko Nakayama**[6], **Hiroyuki Inuzuka**[1,2,*], and **Wenyi Wei**[1,*]

[1]Department of Pathology, Beth Israel Deaconess Medical Center, Harvard Medical School, Boston, MA 02215, USA

[2]Center for Advanced Stem Cell and Regenerative Research, Tohoku University Graduate School of Dentistry, Sendai 980-8575, Japan

[3]Department of Infectious Diseases, National Center for Global Health and Medicine, Tokyo 162-8655, Japan

[4]Cell Signaling Technology, Inc., Danvers, MA 01923, USA

[5]Department of Physiological Sciences and Molecular Biology, Fukuoka Dental College, Fukuoka 814-0193, Japan

[6]Division of Cell Proliferation, ART, Graduate School of Medicine, Tohoku University, Sendai 980-8575, Japan

[7]Division of Pediatric Dentistry, Department of Oral Health and Development Sciences, Tohoku University Graduate School of Dentistry, Sendai 980-8575, Japan

[8]Division of Signal Transduction, Beth Israel Deaconess Medical Center and Department of Medicine, Harvard Medical School, Boston, MA 02115, USA

[9]Division of Cell Regulation Systems, Medical Institute of Bioregulation, Kyushu University, Fukuoka 812-8582, Japan

Abstract

[*]Corresponding author: hinuzuka@bidmc.harvard.edu (H.I.); wwei2@bidmc.harvard.edu (W.W.).
[†]These authors contributed equally to this work.

Author contributions: K.S. and H.F. designed and performed most of the experiments with assistance from K.O., N.T.N., J.Z., B.J.N., A.G., K.N., T.N., S.H., A.W., and H.I.. J.M.A. performed the mass spectrometry analysis and E.C.L. analyzed the data. K.O., A.Y., S.F., K.I.N., K.N., A.T., H.I., and W.W. guided and supervised the study. K.S., H.F., H.I., and W.W. wrote the manuscript. All authors commented on the manuscript

Competing interests: The authors declare that they have no competing interests.

Data and materials availability: The mass spectrometry phosphoproteomics data have been deposited to the PhosphoSite database (http://www.phosphosite.org/staticSupp.action#supp). The data are located within the “Supplementary Data For High Throughput Protein Modification Publications from Cell Signaling Technology” (http://www.phosphosite.org/suppData/Kouhei/Phosphoproteomic-data_Web-linked_DSGXXS.xlsx; http://www.phosphosite.org/suppData/Kouhei/Phosphoproteomic-data_Web-linked_DSGXXXS.xlsx).

The $SCF^{\beta\text{-}TRCP}$ E3 ubiquitin ligase complex plays pivotal roles in normal cellular physiology and in pathophysiological conditions. Identification of β-transducin repeat-containing protein (β-TRCP) substrates is therefore critical to understand $SCF^{\beta\text{-}TRCP}$ biology and function. Here, we used a β-TRCP-phosphodegron-motif specific antibody in a β-TRCP substrate screen coupled with tandem mass spectrometry and identified multiple β-TRCP substrates. One of these substrates was Lipin1, an enzyme and suppressor of the family of sterol regulatory element-binding protein (SREBP) transcription factors, which activate genes encoding lipogenic factors. We showed that $SCF^{\beta\text{-}TRCP}$ specifically interacted with and promoted the polyubiquitination of Lipin1 in a manner that required phosphorylation of Lipin1 by mechanistic target of rapamycin 1 (mTORC1) and casein kinase I (CKI). *β-TRCP* depletion in HepG2 hepatocellular carcinoma cells resulted in increased Lipin1 protein abundance, suppression of SREBP-dependent gene expression, and attenuation of triglyceride synthesis. Moreover, *β-TRCP1* knockout mice showed increased Lipin1 protein abundance and were protected from hepatic steatosis induced by a high-fat diet. Together, these data reveal a critical physiological function of β-TRCP in regulating hepatic lipid metabolic homeostasis in part through modulating Lipin1 stability.

Introduction

Energy imbalance leads to increased weight gain and obesity. These pathological conditions increase the risk of developing type 2 diabetes, cardiovascular disease, hypertension, stroke and cancer (1). Metabolic risk factors such as obesity, type 2 diabetes mellitus, and dyslipidemia contribute to the development of fatty liver disease (2), which is a potential cause of liver cirrhosis, liver failure, and ultimately hepatocellular carcinoma (3, 4). Although metabolic syndrome is thought to be a major cause of fatty liver disorders, its physiological role in the development of liver steatosis and steatohepatitis remains unclear.

The ubiquitin-proteasome system (UPS) governs diverse cellular processes including, but not limited to, cell cycle progression, cell differentiation, and development (5, 6). The UPS consists of three discrete enzymes: E1 ubiquitin-activating enzymes, E2 ubiquitin-conjugating enzymes and E3 ubiquitin ligases. E3 ligases covalently attach ubiquitin molecules to target proteins for subsequent degradation by the 26S proteasome. There are estimated to be over 600 E3 ligases in the human genome, thereby providing the necessary diversity to confer substrate specificity in the UPS enzyme cascade reaction (7, 8). E3 ligases are further categorized into three major groups: HECT, RING and PHD/U-box. Among these, RING-type E3 ligases constitute the largest group and are further subdivided into two major categories: single-subunit RING proteins and the multi-subunit RING-type E3 complexes. Notably, the SCF (Skp1-Cullin1-F-box protein) E3 ligase complex is a well-characterized multi-subunit RING-type E3 ligase that functions as a major regulator of various cellular processes including cell cycle, cell apoptosis and metabolism (9–11).

The SCF complex comprises four core subunits: the RING subunit Ring box protein 1 (Rbx1), the scaffold subunit Cullin 1, the adaptor subunit Skp1 and a substrate receptor subunit F-box protein (11, 12). To date, 69 putative F-box proteins have been identified in the human genome (13). SCF complexes exhibit diverse substrate specificity because of the use of variable F-box proteins as the substrate receptor module that recognizes and recruits

specific substrates to the SCF catalytic core (14). The F-box protein β-TRCP has two distinct paralogs, β-TRCP1 (also termed F-box/WD repeat-containing protein 1A: FBXW1) and β-TRCP2 (also termed F-box/WD repeat-containing protein 11: FBXW11) that share identical biological and biochemical traits (15). β-TRCP regulates many cellular processes by targeting diverse substrates such as nuclear factor kappa B (NF-κB)/inhibitor of kappa B (IκB) proteins (16), early mitotic inhibitor 1 (Emi1) (17), cell division cycle 25 homologue A (Cdc25A) (18, 19), vascular endothelial growth factor receptor 2 (VEGFR2) (20), DEP domain-containing mTOR-interacting protein (DEPTOR) (21) and SET domain-containing protein 8 (Set8) (22), for proteasome-mediated degradation. Although β-TRCP substrates continue to be identified, it is predicted that a large number of substrates have yet to be discovered which mediate crucial roles in physiology and pathology. To this end, affinity purification-based strategies have been widely employed for identification of β-TRCP substrates, although most of them rely on methods based on ectopic overexpression that may lead to unexpected artificial and non-specific interactions due to non-physiological experimental conditions.

The consensus β-TRCP degron sequence is defined as DSGxxS, where Ser residues must be phosphorylated for β-TRCP to accurately recognize the motif (23). In the present study, we developed anti-β-TRCP-phospho-degron motif antibodies for an immunoaffinity-purification screening approach coupled with mass-spectrometry to identify new β-TRCP substrates. Our goal was to identify β-TRCP substrates with both low abundance and low affinity for the substrate recognition pocket of β-TRCP. Using this screen, we identified many previously-described β-TRCP substrates, thus validating the approach. Furthermore, we have discovered several new β-TRCP candidate substrates that contain a phosphorylated β-TRCP degron motif, such as Lipin1, an enzyme critical for lipid metabolism and homeostasis.

Lipin1 regulates metabolic and energy homeostasis (24). The *Lpin1* genetic rearrangement leading to a null mutation or a naturally-occurring point mutation contributes to the phenotype of neonatal fatty liver dystrophy (fld) in *fld and fld*^{2j} mice, respectively (25). *Fld* mice display various pathophysiological traits such as neonatal fatty liver, hypertriglyceridemia, insulin resistance, peripheral neuropathy and lipodystrophy (26, 27), highlighting a pivotal role for Lipin1 in lipid homeostasis. Biochemically, Lipin1 is a multifunctional protein with phosphatidate phosphatase (PAP) activity and functions in transcriptional co-regulation (28–31). Specifically, Lipin1 modulates lipid metabolic regulation in part through catalyzing the synthesis of diacylglyceride (DAG) through PAP activity, and also enhancing fatty acid oxidation through transcriptional co-activation of PPARα and PGC-1α. Notably, Lipin1 also has critical roles in the transcriptional regulation of hepatic lipogenesis in the nucleus (29, 32–34) largely by suppressing the functions of the SREBP family of transcription factors, a mater regulator that governs fatty acid and cholesterol biosynthetic gene expression (35). Specifically, nuclear Lipin1 inhibits SREBP-dependent gene transcription when the mTORC1 signaling pathway is inactive. Mechanistically, phosphorylation by mTORC1 inhibits nuclear accumulation of Lipin1, which in turn induces transcriptional activation of SREBP target genes (34).

Here, we report that polyubiquitination of Lipin1 is targeted by β-TRCP in a CKI-dependent manner. We further demonstrate that β-TRCP regulates hepatic lipid metabolism by controlling Lipin1 protein stability. Our study highlights a new physiological function of β-TRCP in regulating hepatic lipogenesis in part through controlling Lipin1 stability.

Results

Screening based on phospho-degron antibody-mediated mass spectrometry enables identification of substrates of $SCF^{\beta\text{-}TRCP}$ E3 ligase complex

The majority of characterized F-box proteins recognize degron motifs within target proteins, typically in combination with post-translational modification of the degron motifs such as phosphorylation, acetylation, methylation or glycosylation (10, 11). Because β-TRCP recognizes a specific phosphorylated degron (phospho-degron) motif, we designed an immuno-purification-based screening strategy to efficiently capture β-TRCP substrates in combination with microcapillary liquid chromatography - tandem mass spectrometry (LC-MS/MS) (fig. S1A). To this end, we developed specific antibodies that recognized the β-TRCP consensus phospho-degron motifs DpSGxxpS and DpSGxxxpS, respectively.

We first validated the specificity of these antibodies in recognizing previously-identified β-TRCP consensus motifs including those in mouse double minute 2 (Mdm2) (36), NF-κB1 (37), ubiquitin like with PHD and ring finger domains 1 (UHRF1) (38) and metastasis suppressor 1 (MTSS1) (39). Using a peptide dot-blot assay, we confirmed that these β-TRCP phospho-degron motif antibodies specifically recognized the degron motif of Mdm2 when Ser^{118} and Ser^{121} were phosphorylated (fig. S1B). Accordingly, these antibodies reacted with the phospho-degron motif of ectopically expressed wild-type Mdm2, but not the S118A/S121A mutant (fig. S1C). Similarly, we evaluated antibody specificity using additional reported β-TRCP motifs in NF-κB1, UHRF1 and MTSS1 (Fig. 1, A to C). Mutating Ser residues to Ala within the individual degron sequences of these β-TRCP substrates abolished antibody reactivity (Fig. 1, A to C). Together, these results confirm the antibody specificity. However, we noted that under our experimental conditions, the first Ser residue within the DSG motif in β-TRCP phospho-degron was more critical for recognition by our antibodies.

We next sought to identify potential β-TRCP substrates in Jurkat and OVCAR5 cells. To block degradation of β-TRCP substrate proteins by the 26S proteasome, cells were pretreated with MG132 and subsequently harvested and subjected to tryptic digestion. Tryptic peptides were then subjected to immunoprecipitation with anti-β-TRCP degron motif antibodies (fig. S1A). The enriched phospho-peptides from the immunoprecipitation were analyzed by LC-MS/MS. Using this approach, we detected previously characterized β-TRCP substrates including β-catenin (CTNNB1), IκBs, NF-κB1 and programmed cell death 4 (PDCD4) (table S1). In addition to these known substrates, we identified additional 93 putative β-TRCP substrates that contain the DSG motif in which the core Ser residue was phosphorylated in cells.

We validated sixteen candidate proteins for which specific antibodies are commercially available by examining their accumulation following depletion of *β-TRCP1* and/or *β-*

TRCP2 in HeLa cells. Among these, we found that the protein abundance of Lipin1, alkaline phosphatase (ALPP), Lysine-rich CEACAM1 co-isolated protein (Lyric), and protein activator of the interferon-induced protein kinase (PACT) was substantially increased in *β-TRCP* depleted cells (Fig. 1D, and table S1), while the mRNA abundance of *LPIN1*, *ALPP*, *MTDH* (*Lyric*), or *PACT* was minimally affected (fig. S1D). Moreover, the anti-β-TRCP phospho-degron antibodies recognized the β-TRCP degron motifs of β-TRCP substrates when ectopically expressed in cells, and mutation of key Ser residues within the degron abolished the signal (Fig. 1, E to H). These data demonstrate that these antibodies captured putative β-TRCP degron motif-containing peptides and proteins and identified β-TRCP downstream ubiquitin substrates.

We then examined whether Lipin1, ALPP, Lyric, and PACT were bona fide substrates of $SCF^{\beta\text{-}TRCP}$ E3 ligase complex. Consistent with the evolutionary conservation of β-TRCP degron motifs in these candidates across different species (Fig. 2, A to D), co-immunoprecipitation experiments showed that their interaction with β-TRCP was largely abolished when the key Ser residues in the β-TRCP recognition motifs were mutated (Fig. 2, E to H). The interaction between β-TRCP and individual putative substrates was also abolished when the substrate recognition domain of β-TRCP was mutated to R474A (40), thus further confirming binding specificity (fig. S2, A to D). Moreover, β-TRCP-induced polyubiquitination of these candidate proteins occurred in a phospho-degron-dependent manner in cells (Fig. 2, I to L), corroborating the notion that $SCF^{\beta\text{-}TRCP}$ is a bona fide E3 ligase of Lipin1, ALPP, Lyric, and PACT.

The $SCF^{\beta\text{-}TRCP}$ E3 ligase complex associates with Lipin1 to control its protein stability

We focused our subsequent analysis on Lipin1, a critical regulator of lipid homeostasis (24, 41), since this could potentially reveal an important link between the physiological function of β-TRCP and cellular metabolism. In further support of Lipin1 as a specific β-TRCP substrate, we found that Lipin1 specifically interacted with β-TRCP1, but not any of the other F-box proteins tested (Fig. 3A). Furthermore, the Lipin1 and β-TRCP1 interaction was detected endogenously, suggesting that the regulation of Lipin1 by β-TRCP1 could be physiologically important (Fig. 3B).

We next showed that Lipin1 specifically interacted with Cullin1, a scaffolding subunit of the $SCF^{\beta\text{-}TRCP}$ E3 ligase complex, but not other related Cullin family members tested (Fig. 3C). This process likely functioned through recognition of the phospho-degron of Lipin1 by β-TRCP, as the interaction between Cullin1 and Lipin1 was abolished by mutation of the Lipin1 degron (fig. S3A). Moreover, depletion of *Cullin1* resulted in accumulation of Lipin1 protein (Fig. 3D), suggesting a possible role for Cullin1 in controlling Lipin1 protein stability. The increase in Lipin1 abundance induced by depletion of *β-TRCP* (Fig. 1D) in HeLa cells was mediated by an extension in the half-life of endogenous Lipin1 protein (Fig. 3, E and F). Consistent with these data, mutating Ser^{483} and Ser^{487} to Ala within the degron motif in Lipin1, which disrupted the interaction between Lipin1 and the $SCF^{\beta\text{-}TRCP}$ complex, also extended the half-life of Lipin1 protein (fig. S3, B and C). Together, these results support our model that Lipin1 is a bona fide substrate of the $SCF^{\beta\text{-}TRCP}$ complex.

To further understand the molecular basis of Lipin1 ubiquitination, we attempted to identify the ubiquitination site(s) mediated by β-TRCP. To this end, we focused on the previously reported sumoylation sites (Lys^{599} and Lys^{629}) (42) and ubiquitination site (Lys^{804}) (PhosphoSite, http://www.phosphosite.org/siteAction.action?id=12289775) because sumoylation and ubiquitination can target the same lysine residues (43). The cellular ubiquitination assay demonstrated that the polyubiquitination of K804R-Lipin1 directed by β-TRCP was decreased in cells (fig. S3D), suggesting that Lys^{804} might be the major β-TRCP-mediated ubiquitination site in Lipin1.

Casein Kinase I (CKI) phosphorylates the degron motif in Lipin1 to trigger its interaction with β-TRCP

β-TRCP typically recognizes substrates with phosphorylated Ser residues within the degron motif (DSGxxS) (15). To identify the upstream kinase for the Lipin1 degron, we ectopically expressed Lipin1 with a panel of protein kinases including CKI, glycogen synthase kinase 3β (GSK3β), and ribosomal protein S6 kinase B1 (S6K1), which participate in priming β-TRCP phospho-degrons (11). Notably, the abundance of ectopically expressed Lipin1 was decreased by co-expression of casein kinase I isoforms (CKIα, δ and ε) (fig. S4A). Conversely, endogenous Lipin1 protein abundance was increased by treatment with the CKI inhibitor D4476 (20, 44) (Fig. 4A). Moreover, treatment with D4476 diminished phosphorylation at the β-TRCP1 consensus degron in Lipin1 (Fig. 4B), leading to a reduced interaction between Lipin1 and β-TRCP1 (Fig. 4C).

We next determined the specific CKI isoform responsible for regulating the Lipin1/β-TRCP interaction. CKIε preferentially associated with Lipin1 compared to other CKI isoforms including CKIα and CKIδ (Fig. 4D). Furthermore, depletion of endogenous *CKIε*, but not *CKIα* or *CKIδ*, resulted in accumulation of endogenous Lipin1 (Fig. 4E), suggesting that CKIε plays a major physiological role in controlling Lipin1 stability. Similarly, the protein half-life of endogenous Lipin1 was markedly prolonged upon *CKIε* depletion (Fig. 4, F and G). Treatment of glutathione S-transferase (GST)-tagged Lipin1 with recombinant CKI promoted the interaction between β-TRCP1 and GST-Lipin1 in vitro in a phosphorylation-dependent manner, whereas mutation of the Ser residues within the β-TRCP degron motif (Ser^{483} and Ser^{487}) to Ala abolished this interaction (Fig. 4H).

In vitro ubiquitination assays revealed that recombinant CKI enhanced the β-TRCP-dependent polyubiquitination of wild-type Lipin1 to a greater extent than that of the S483A/S487A phospho-degron mutant (Fig. 4I). Similarly, D4476 suppressed Lipin1 ubiquitination (Fig. 4J), and ectopic expression of CKI destabilized wild-type Lipin1, but not the S483A/S487A mutant (fig. S4, B and C). These data together demonstrate that CKI is a major modifying kinase for Lipin1 and controls protein stability through β-TRCP interaction.

β-TRCP controls Lipin1 stability to govern its suppression of SREBP-dependent transcription

Lipin1 suppresses SREBP-dependent transcription (34). We therefore next measured alterations in SREBP target genes after depletion of *β-TRCP*. Consistent with a role in regulating Lipin1 stability and function, the transcript abundance of SREBP target genes was

decreased in *β-TRCP* depleted cells, although SREBP protein abundance was not altered (Fig. 5, A and B). Furthermore, when compared to wild-type Lipin1, the S483A/S487A Lipin1 mutant was more potent at suppressing SREBP transcriptional activity (Fig. 5C, and fig. S5, A and B). SREBP promoter activity was further suppressed after depleting *β-TRCP1* in cells expressing wild-type Lipin1, but not in cells expressing the S483A/S487A mutant (Fig. 5C). SREBP target gene expression was significantly decreased following *β-TRCP* depletion in cells expressing wild-type Lipin1, but not the S483A/S487A mutant (Fig. 5D). This phenotype appears to be related to the stabilization of wild-type Lipin1 protein abundance following *β-TRCP* depletion (Fig. 5E).

In agreement with a pivotal role for CKI in priming Lipin1 for degradation by β-TRCP1 (Fig. 4), treatment with D4476 reduced SREBP1 transcriptional activity (fig. S5C). D4476 did not significantly affect SREBP1 transcriptional activity in *β-TRCP1*-depleted cells, supporting a model in which β-TRCP and CKI coordinately regulate Lipin1 (Fig. 5F). Together, the above findings suggest that β-TRCP regulates SREBP largely through controlling Lipin1 abundance in collaboration with the upstream modifying enzyme CKI.

β-TRCP controls lipogenesis in a Lipin1-dependent manner in hepatocytes

Lipin1 has critical roles in the transcriptional regulation of hepatic lipogenesis in the nucleus (29, 32, 33), and inhibits the transcriptional activity of the active form of SREBP (34). Therefore, we next investigated the importance of Lipin1 degradation by β-TRCP in hepatic lipid metabolism. *β-TRCP* depletion in HepG2 cells triggered the accumulation of Lipin1 (Fig. 6A), indicating that in hepatocytes, Lipin1 protein stability was also regulated by $SCF^{β\text{-}TRCP}$-mediated ubiquitination. Furthermore, depletion of *β-TRCP1* or *β-TRCP2* led to decreased SREBP transcriptional activity (Fig. 6, B and C), whereas knockdown of both *LPIN1* and *β-TRCP* restored SREBP activity (Fig. 6, B and C, and fig. S6, A and B). These findings suggest that $SCF^{β\text{-}TRCP}$ governed SREBP activity largely through the Lipin1 pathway.

Next, to evaluate the effects of *β-TRCP* depletion in hepatic lipid synthesis, we analyzed triglyceride content in *β-TRCP*-depleted HepG2 cells. Triglyceride content was markedly decreased following *β-TRCP* knockdown, and was partially restored following depletion of *LPIN1* (Fig. 6, D and E). Lipidomics analysis of hepatocytes by shotgun LC-MS/MS using positive/negative switching and LipidSearch software (45) demonstrated that the amounts of nearly all of the triglyceride species were significantly decreased following *β-TRCP1* knockdown (Fig. 6F). These data suggest that β-TRCP enhanced hepatic lipogenesis in part by decreasing protein abundance of Lipin1, an inhibitor of hepatic lipogenesis (34).

mTORC1 activity promotes CKI and β-TRCP-dependent Lipin1 ubiquitination

The mTORC1 pathway drives lipogenesis by enhancing SREBP activity (46–48). Phosphorylation of Lipin1 by mTORC1 blocks its nuclear accumulation, leading to increased expression of SREBP-dependent genes encoding lipogenic factors (34). Our studies showed that β-TRCP degraded Lipin1 to activate hepatic lipogenic gene expression, likely by enhancing SREBP transcriptional activity. These data suggest that β-TRCP/Lipin1 signaling could function as a critical mediator between mTORC1 and SREBP for lipogenic

gene expression (Fig. 7A). In support of this model, we observed that the mTORC1 signaling pathway modulated β-TRCP1-mediated Lipin1 degradation. The phosphorylation deficient Lipin1 mutant, in which all 21 reported phosphorylation sites including seven proline-directed sites (S/T-P) that can be phosphorylated by mTORC1 are substituted with Ala except for Ser^{483} (mTORC1ΔST) (34), displayed a significant decrease in the phosphorylation of the β-TRCP degron motif compared to wild-type Lipin1 (Fig. 7B and fig. S7), resulting in diminished association between Lipin1 and β-TRCP1 (Fig. 7C).

Consistent with this model, pharmacological blockade of mTORC1 with Torin1 resulted in diminished phosphorylation of Ser^{483} and Ser^{487} (Fig. 7D) and abolished the interaction between β-TRCP1 and Lipin1 (Fig. 7E), leading to abrogation of Lipin1 ubiquitination (Fig. 7F) and extended Lipin1 half-life (Fig. 7, G and H). These results suggest that the mTORC1-mediated Lipin1 modification may allow CKI to phosphorylate Ser residues within the β-TRCP degron in Lipin1. In addition, Lipin1 abundance was increased under serum-starved conditions (Fig. 7I), probably due to diminished mTORC1 activity and subsequent dissociation of Lipin1 from β-TRCP. In agreement with this finding, depletion of endogenous *β-TRCP1* failed to induce an increase in Lipin1 protein abundance in serum starved-cells (Fig. 7I), supporting the model that the CKI/β-TRCP signaling pathway modulates nutrition-dependent control of Lipin1 expression (Fig. 7A).

Together, these data imply that mTORC1 may serve as a priming kinase for CKI to efficiently promote β-TRCP-mediated Lipin1 degradation, which in turn activates SREBP transcriptional activity (Fig. 7A). β-TRCP degrades the mTOR inhibitor DEPTOR (21, 49, 50), supporting a model that β-TRCP may be a key regulator of multiple key components in lipogenesis.

β-TRCP1 (Btrc) knockout mice are protected from high fat diet-induced hepatic steatosis

We assessed the physiological roles of β-TRCP in hepatic lipid homeostasis in vivo using *β-TRCP1*$^{-/-}$ mice (51). Although there was a trend for *β-TRCP1*$^{-/-}$ mice to gain less weight than wild-type mice in response to high fat diet (HFD), these differences did not reach statistical significance (fig. S8A). However, the livers of HFD-fed *β-TRCP1*$^{-/-}$ mice were reduced in size and mass, and had a less whitish appearance compared with those of wild-type mice (Fig. 8, A and B), suggesting a reduction in fatty liver. Indeed, HFD-fed *β-TRCP1*$^{-/-}$ mice displayed reduced lipid accumulation in livers, while wild-type mice were more susceptible to excess lipid deposits including triglycerides (Fig. 8, C and D), suggesting a critical role of β-TRCP in regulating hepatic lipid metabolism. Moreover, under fasted conditions, the *β-TRCP1*$^{-/-}$ mice on a HFD had lower plasma glucose and insulin concentrations than wild-type mice on a HFD (fig. S8, B and C), suggesting that the *β-TRCP1*$^{-/-}$ mice were less insulin resistant.

Consistent with results obtained in several cell lines including HepG2 cells, Lipin1 protein abundance in livers was increased in *β-TRCP1*$^{-/-}$ mice fed with a HFD, and to a lesser extent with normal diet (ND) (Fig. 8E). To assess the molecular mechanism by which β-TRCP/Lipin1 signaling regulates lipogenesis in hepatocytes, we further investigated the transcript abundance of SREBP target genes in liver. Notably, under HFD conditions, the expression of various SREBP target genes in the liver was decreased in *β-TRCP1*$^{-/-}$ mice

compared with the wild-type mice (Fig. 8F), suggesting a possible molecular mechanism for Lipin1-mediated suppression of SREBP transcriptional activity in governing the reduced development of hepatic steatosis in *β-TRCP1*$^{-/-}$ mice in a high-fat diet. However, abrogation of *β-TRCP1* did not affect expression of lipogenic genes in response to normal diet intake under fasting-refeeding condition (fig. S8D). Together, our data indicate that β-TRCP plays an important role in regulating lipid homeostasis in vivo in part through controlling Lipin1 protein stability, and deregulation of β-TRCP function may contribute to developing HFD-induced hepatic steatosis.

Discussion

To date, numerous approaches have been used to identify substrates of β-TRCP (21, 52–56). In our study, we set out to identify additional β-TRCP substrates with a newly-developed antibody that specifically recognized the phospho-degron motif utilized by β-TRCP. Immunoprecipitating lysates with this phospho-degron-motif antibody followed by LC-MS/MS analysis identified a large set of putative β-TRCP substrates. Of the 93 putative substrates identified, we selected 16 to determine if their protein abundance was regulated by *β-TRCP* depletion, and found four (Lipin1, ALPP, Lyric, and PACT) that are likely bona fide β-TRCP substrates. However, 12 proteins did not show increased abundance upon *β-TRCP* depletion, a possible indication that either these proteins are not Lys^{48}-linked β-TRCP substrates, that they are not properly phosphorylated to a sufficient stoichiometry under the experimental conditions utilized, or that they require additional regulatory modifications to allow recognition and degradation by β-TRCP. Therefore, additional analysis of these putative targets, as well as the remaining 80 untested substrates, is required to determine if they are true physiological β-TRCP substrates or β-TRCP-interacting proteins.

We focused our analysis on Lipin1, a key regulator of lipid homeostasis, as a substrate for β-TRCP. We showed that β-TRCP interacted with Lipin1 through the WD40 repeats domain of β-TRCP and the degron motif in Lipin1. We further showed that β-TRCP required CKI-mediated phosphorylation of Ser residues within the degron motif for targeting Lipin1. Moreover, we found that blocking mTOR kinase activity also abolished β-TRCP interaction with Lipin1 in part by reducing the phosphorylation of the Ser residues within the degron motif. Thus, we propose that mTORC1 may function as a priming kinase for CKI to promote the phosphorylation of the degron motif in Lipin1. Because CKI is a constitutively active kinase and ubiquitously distributed in many cell types, high mTORC1 activity depending on nutritional status may be a physiological cue for Lipin1 degradation mediated by CKI and β-TRCP.

CKI plays important roles in regulating several metabolic pathways through phosphorylation of the key regulators peroxisome proliferator-activated receptor-γ co-activator 1α (PGC-1α) and N-terminal transcription factor domain of Sre1 (Sre1N), a yeast homolog of active SREBP, for proteasome dependent degradation (57, 58). In addition, CKIδ-mediated phosphorylation of hypoxia-inducible factor 1α (HIF-1α) suppresses HIF-1α-dependent *LPIN1* mRNA expression, leading to a decrease in lipid synthesis under hypoxia. (59). Here, we showed that CKIε contributed to lipid metabolism through controlling Lipin1 stability,

specifically by mediating the priming phosphorylation of the β-TRCP degron motif in Lipin1. Consistent with a role of CKI/β-TRCP in regulating Lipin1 stability, depletion of *β-TRCP* or inhibition of CKI led to a decrease in the SREBP transcriptional function. CKI/β-TRCP signaling plays a crucial role in circadian pace-making by directly targeting period circadian clock (PER) and cryptochrome (CRY) for degradation (60). Because disrupted circadian rhythms lead to various metabolic syndromes such as obesity and diabetes, our data may also imply that the CKI/β-TRCP/Lipin1 pathway contributes to the interrelationship between circadian oscillation and lipid metabolism. Therefore, our results may suggest a role for CKI/β-TRCP in regulating lipogenesis by promoting the degradation of Lipin1.

This study linked $SCF^{\beta\text{-}TRCP}$ E3 ligase activity to cellular metabolism. However, Lipin1 appears to play paradoxical dual roles in maintaining cellular lipid metabolism: In the cytoplasm, Lipin1 catalyzes triglyceride synthesis through enzymatic PAP activity, whereas Lipin1 also controls the expression of genes that mediate fatty acid oxidation and lipogenesis through transcriptional co-activator or co-repressor functions in the nucleus (61). Lipin1 has been suggested to exert distinct roles in controlling lipogenesis and energy metabolism in a context-dependent or tissue-specific manner. For example, the PAP activity of Lipin1 is essential for adipocyte differentiation (62, 63). In contrast, the PAP activity of Lipin1 may not be important for increasing hepatic triglyceride content (27), and instead, its transcriptional regulator function may contribute to hepatic lipid homeostasis (29, 32, 33).

Our data suggest that β-TRCP promotes hepatic lipogenesis by Lipin1 degradation and subsequent deregulation of SREBP-dependent transcription, thereby providing mechanistic insight into the role of β-TRCP in hepatic lipid homeostasis. Future studies investigating tissue-specific functions of the β-TRCP/Lipin1 signaling pathway, such as in adipocytes and skeletal muscle, will be of interest since transgenic mice overexpressing Lipin1 in these tissues develop obesity (64). The *β-TRCP1/2* double knockout mice in lipogenic tissues such as adipose, skeletal muscle and liver could also provide further evidence that β-TRCP has critical roles in lipid homeostasis in a tissue-restricted manner. In this study, we observed no substantial differences between wild-type and $\beta\text{-}TRCP1^{-/-}$ mice in body weight, fasting glucose concentration and fasting insulin concentration, under normal diet conditions (fig. S8, A to C), and in the expression of SREBP target genes under fasting-refeeding conditions (fig. S8D). These results imply that the β-TRCP/Lipin1 signaling may minimally contribute to regulating systemic metabolism under normal metabolic conditions. Instead, the Lipin1 degradation pathway may play a more critical role under various metabolic stress conditions such as HFD or obesity.

In summary, we identified multiple β-TRCP substrates using an immunoaffinity approach and further validated Lipin1, a critical modulator of lipid homeostasis, as a bona fide β-TRCP substrate. Since aberrant signaling involving the β-TRCP/Lipin1 pathway may lead to various metabolic symptoms, our results provide insight into potential new therapeutic interventions for metabolic syndrome caused by compromised Lipin1 stability.

Materials and Methods

Cell Culture

293T, HeLa, NIH-3T3, OVCAR-5 and MDA-MB-231 cells were maintained in Dulbecco's Modified Eagle Medium (DMEM) medium. Jurkat cells and HepG2 cells were maintained in Roswell Park Memorial Institute (RPMI) 1640 and Minimum Essential Medium (MEM), respectively. Each medium was supplemented with 10% fetal bovine serum (FBS), 100 Units of penicillin and 100 μg/ml streptomycin. Cell transfection was performed as described previously (65). Packaging of lentiviruses, retroviruses, and subsequent infection of various cell lines were performed according to the protocol described previously (66, 67). Following viral infection, cells were selected for at least 72 h in the presence of puromycin (1 μg/ml) or hygromycin (200 μg/ml), depending on the viral vectors used to infect cells. Cycloheximide (CHX) was used at 100 μg/ml for the indicated time periods.

Antibodies

Anti-A-kinase anchor protein 11 (AKAP11) antibody (610704) was purchased from BD Bioscience. Anti-zinc finger protein 148 (ZNF148) antibody (A303-117A-1), anti-acyl-CoA-binding domain-containing protein 5 (ACBD5) antibody (A303-296A-1), anti-adducin 1 (ADD1) antibody (A303-713A-1), anti-kinesin family member 1C (KIF1C) antibody (A301-072A-1), anti-MYST histone acetyltransferase 2 (MYST2) antibody (A302-225A-1), anti-ribonucleoprotein PTB-binding 1 (RAVER1) antibody (A303-939A-1), and anti-RNA binding motif protein 6 (RBM6) antibody (A301-013A) were purchased from Bethyl Laboratories. Monoclonal anti-human influenza hemagglutinin (HA) antibody (MMS-101P) was purchased from Covance. Anti-ALPP antibody (8681), anti-Lyric antibody (9596), anti-PACT antibody (11277), anti-N-alpha-acetyltransferase 10 (NAA10) antibody (9046), anti-Nuclear mitotic apparatus protein 1 (NuMA-1) antibody (3888), polyclonal anti-Myc-Tag antibody (2278), monoclonal anti-Myc-Tag antibody (2276), anti-β-TRCP1 antibody (4394), and anti-GST antibody (2625) were purchased from Cell Signaling Technology. Anti-Lipin1 antibody (sc-376874), anti-MAPK/ERK kinase kinase 1 (MEKK1) antibody (sc-449), anti-Cdc25A antibody (sc-7389), anti-CUL1 antibody (sc-11384), anti-Cyclin E antibody (sc-247), anti-cyclin-dependent kinase inhibitor 1B (p27, Kip1) antibody (sc-527), anti-CK1α antibody (sc-6477), anti-CK1δ antibody (sc-6474), anti-CK1ε antibody (sc-6471), anti-SREBP1 antibody (sc-8984), and polyclonal anti-HA antibody (sc-805) were purchased from Santa Cruz. Anti-green fluorescent protein (GFP) antibody (632381) was purchased from Clontech. Anti-Tubulin antibody (T-5168), β-catenin antibody (C-7207), polyclonal anti-Flag antibody (F-2425), monoclonal anti-Flag antibody (F-3165, clone M2), anti-Flag agarose beads (A-2220), anti-HA agarose beads (A-2095), peroxidase-conjugated anti-mouse secondary antibody (A-4416), and peroxidase-conjugated anti-rabbit secondary antibody (A-4914) were purchased from Sigma. Anti-DpSGxxpS and anti-DpSGxxxpS motif antibodies were generated in collaboration with Cell Signaling Technology.

Plasmids

pRK-FLAG-mouse Lipin1 (Flag-Lipin1) was purchased from Addgene (32005). GST-Lipin1 (420–623 aa) and pBabe-Flag-Lipin1 were constructed by inserting the corresponding cDNA into pGEX-4T-1 and pBabe-hygro vectors, respectively. CMV-ALPP

(human) was purchased from Addgene (24595) and the ALPP cDNA was subcloned into pCMV-Flag and pCMV-GST. pCMV6-Flag-Myc-Lyric (human) plasmid was kindly provided by Dr. Xiangbing Meng. HA-NFκB1 was generated by inserting human NFκB1 cDNA into pcDNA3-HA. Flag-UHRF1 expression plasmid was described previously (38). Myc-MTSS1 was described previously (39). pcDNA3-PACT (human) plasmid was purchased from Addgene (15667) and the PACT cDNA was subcloned into pcDNA3-HA. shβ-TRCP1 (mouse) was purchased from Open Biosystems. shLipin1 (mouse and human) plasmids were constructed by inserting annealed oligos designed in (34) into pLKO-puro. HA-Mdm2, HA-β-TRCP1, Flag-β-TRCP1, Myc-β-TRCP1, Myc-β-TRCP2, GST-F-box proteins, Myc-CKI isoforms, Flag-CKIIα, Myc-Cullin isoforms and shRNA constructs against *GFP*, *β-TRCP1*, *β-TRCP2*, *β-TRCP1+2*, *Cullin1* and *CKI* isoforms were described previously (21, 36, 68).

Immunoblots and Immunoprecipitation

Cells were lysed in EBC buffer (50 mM Tris pH 7.5, 120 mM NaCl, 0.5% NP-40) supplemented with protease inhibitors (Complete Mini, Roche) and phosphatase inhibitors (Calbiochem 524624 and 524625). The protein concentrations of lysates were measured by the Beckman Coulter DU-800 spectrophotometer using the Bio-Rad protein assay reagent. Same amounts of whole cell lysates were resolved by sodium dodecyl sulfate polyacrylamide gel electrophoresis (SDS-PAGE) and immunoblotted with indicated antibodies. For immunoprecipitation, cells were treated with MG132 (15 μM) in the absence or presence of D4476 (20 μM) or Torin1 (250 nM) overnight before harvesting. 1 mg lysates were incubated with the indicated antibodies for 4 h at 4°C followed by 1 h incubation with Protein A sepharose beads (GE Healthcare). Immunoprecipitates were washed five times with NETN buffer (20 mM Tris, pH 8.0, 100 mM NaCl, 1 mM EDTA and 0.5% NP-40) before being resolved by SDS-PAGE and immunoblotted with indicated antibodies.

Cellular Ubiquitination Assays

For β-TRCP1-mediated Lipin1 ubiquitination assays, 293T cells were transfected with the constructs encoding His-Ubiquitin, Flag-Lipin1, HA-β-TRCP1. Twenty-four hours after transfection, cells were treated with MG132 (15 μM) in the absence or presence of D4476 (50 μM) or Torin1 (250 nM) overnight, and then lysed with denatured buffer (6 M guanidine-HCl, 0.1 M Na_2HPO_4/NaH_2PO_4, 10 mM imidazole pH8.0), followed by sonication. After 3 h incubation with Ni-NTA beads (QIAGEN), His-ubiquitinated proteins were purified through 3 times of washes with the denatured buffer and TI buffer (20 mM Tris-HCl, 20 mM imidazole pH6.8), then resolved by SDS-PAGE and immunoblotted with the indicated antibodies.

In Vitro Ubiquitination Assays

The in vitro ubiquitination assays were performed as described previously (69). To purify SCF/β-TRCP1 complex, 293T cells were transfected with vectors encoding GST-β-TRCP1, Myc-Cul-1, Myc-Skp1, and HA-Rbx1. The SCF/β-TRCP1 (E3) complexes were purified from the whole-cell lysates using GST-agarose beads. Before the in vitro ubiquitination assay, indicated GST-Lipin1 proteins were incubated with purified, recombinant active CKI (with kinase reaction buffer as a negative control) in the presence of ATP at 30°C for 30 min.

Afterwards, the kinase reaction products were incubated with purified SCF/β-TRCP1 (E3) complexes in the presence of purified recombinant active E1, E2 (UbcH5a and UbcH3), ATP, and ubiquitin. The reactions were stopped by the addition of 2× SDS-PAGE sample buffer and the reaction products were resolved by SDS-PAGE and probed with the GST antibody.

Real-time RT-PCR Analyses

RNA was extracted using Qiagen RNeasy mini kit, and the reverse transcription reaction was performed using qScript cDNA SuperMix (Quanta Biosciences). The real-time RT-PCR reaction was performed with SYBR Select Master Mix and CFX384 Touch Real-Time PCR Detection System. All procedures were performed according to the manufacturer's instructions. Primers used in this study were listed in Supplementary Table 2.

SREBP-Responsive Promoter Luciferase Assays

NIH-3T3 cells or 293T cells were cotransfected with a renilla luciferase reporter (pRL-TK, Promega) and a firefly luciferase reporter construct driven by an SREBP-1-responsive promoter in a 1:100 ratio, and in combination with HA-SREBP1 construct. Luciferase activities of the cell lysates were measured using Dual-Luciferase Reporter Assay System (Promega) following the manufacturer's instructions. Data were normalized by cellular protein content and renilla luciferase activity.

Determination of Triglyceride Levels in HepG2 Cells

HepG2 cells infected with lentiviral shRNA constructs were selected in 1 μg/ml puromycin for 4 days to eliminate non-infected cells, then harvested by Tris buffer (25 mM, pH 7.6). Relative triglyceride levels of samples were measured with LabAssay Triglyceride kit (Wako) according to manufacturer's instructions. Data were normalized by cellular protein content.

Animals and Animal Care

β-TRCP1$^{-/-}$ knockout mice were a kind gift of Dr. Keiko Nakayama (51). Wild type or *β-TRCP1*$^{-/-}$ knockout male C57BL/6 mice were fed on a high fat diet consisting of 45% of calories from fat (Japan SLC, Inc) starting at 8 weeks of age for 10 weeks. Control mice were fed a standard diet consisting of 4.5% fat (5002 Lab Diet). Unless mentioned in the figure legends, most of the experiments were performed 6 h after withdraw of food. Animals were housed in a specific pathogen-free facility with a 12 h light/12 h dark cycle and given free access to food and water. All animal use was in compliance with the Institute of Laboratory Animal Research Guide for the Care and Use of Laboratory Animals and approved by the University Committee on Use and Care of Animals at the Tohoku University.

Histology and Oil Red O Staining

Tissue was fixed in 10% neutral-buffered formalin (WAKO) at 4 ºC overnight, dehydrated through a graded alcohol series, xylene and paraffin, and embedded in paraffin. Sections of 5 μm were prepared for Haemotoxylin and Eosin (H&E) staining. For Oil Red O staining,

liver tissues, which were frozen in OCT compounds, were cut at 5 μm, mounted on slides and allowed to dry for 1–2 h. The sections were fixed with 10% formalin for 10 min and then the slides were rinsed with PBS (PH 7.4). After air dry, the slides were placed in 100% propylene glycol for 2 min, and stained in 0.5% Oil Red O solution in propylene glycol for 30 min. The slides were transferred to an 85% propylene glycol solution for 1 min., rinsed in distilled water for 2 changes, and processed for hematoxylin counter staining.

Mass Spectrometry Analysis

Protein identification and phosphorylation site mapping were performed after tryptic digestion and analyzed by microcapillary liquid chromatography (C_{18}) tandem mass spectrometry (LC-MS/MS) using a EASY-nLCII nanoflow High Performance Liquid Chromatography (HPLC, from Thermo Fisher Scientific) coupled to a hybrid Orbitrap Elite high resolution mass spectrometer (Thermo Fisher Scientific) in data-dependent acquisition (DDA) positive ion mode at a flow rate of 300 nL/min. Resulting MS/MS data were searched using Mascot 2.5.1 vs the Human protein database (UniProt). Data were imported into Scaffold 4. Software for analysis of protein and peptide identifications including spectral count relative quantification and interpretation of phosphorylation sites. False discovery rates (FDR) using the forward and decoy human database were calculated to be less than 1.0%.

Determination of the Relative Lipid Levels in HepG2 Cells by Mass Spectrometry

HepG2 cells infected with lentiviral shRNA constructs were selected in 1 μg/ml puromycin for 3 days to eliminate non-infected cells, and then harvested by phosphate-buffered saline (PBS) buffer. The cell pellets were homogenized with 20 times volume of chloroform/methanol (2:1 ratio) and agitated with an orbital shaker for 20 min at room temperature. Liquid phase was recovered after centrifugation, and then the solvent was washed with 0.2 volume of 0.9% sodium chloride (NaCl) solution. After vortexing several seconds, the mixture was centrifuged at 2000 rpm to separate into two phases. After removal of the upper phase, the lower chloroform phase containing lipids was evaporated under vacuum in a rotary evaporator.

Lipidomics data were acquired after extraction of non-polar lipids using 2:1 chloroform:methanol and the lower layer was collected and dried. Lipid extracts were re-suspended in 50% methanol/50% IPA and analyzed by liquid chromatography (C_{18}) tandem mass spectrometry (LC-MS/MS) using positive/negative switching with DDA at a flow rate of 260 μL/min. An 1100 HPLC (Agilent) was coupled to a benchtop high resolution QExactive Plus Orbitrap (Thermo Fisher Scientific). Both MS and MS/MS were analyzed for lipid ion identification and relative quantification using LipidSearch 4.16 software.

Statistical Analysis

All quantitative data were presented as the mean ± the standard error of the mean (SEM) or the mean ± the standard deviation (SD) as indicated of at least three independent experiments or biological replicates by Student's *t*-test for between group differences. $p < 0.05$ was considered as statistically significant.

Supplementary Material

Refer to Web version on PubMed Central for supplementary material.

Acknowledgments

We thank Wei lab members and Dr. Hideki Katagiri for critical reading of the manuscript and helpful discussions; M. Yuan and S. Breitkopf for help with mass spectrometry analysis; K. Oka for technical assistance with immunohistochemistry.

Funding: W.W. is supported in part by NIH grants (GM094777 and CA177910) and Chinese NSFC Grants (31528015). W.W. is an ACS research scholar and a LLS research scholar. H.I. is supported by NIH K01 grant (AG041218), the Charles H. Hood Foundation, and Astellas Foundation for Research on Metabolic Disorders. K.S. is supported by The Naito Foundation and The Uehara Memorial Foundation, and H.F. is supported by JSPS Kakenhi grant (26462829). B.J.N. is supported in part by NIH K01 grant AG052627. J.M.A. is supported in part by NIH grants 5P01CA120964, 5P30CA006516 and R35CA197459.

References and Notes

1. Eyre H, et al. Preventing cancer, cardiovascular disease, and diabetes: a common agenda for the American Cancer Society, the American Diabetes Association, and the American Heart Association. Circulation. 2004; 109:3244–3255. [PubMed: 15198946]
2. Chalasani N, et al. The diagnosis and management of non-alcoholic fatty liver disease: practice Guideline by the American Association for the Study of Liver Diseases, American College of Gastroenterology, and the American Gastroenterological Association. Hepatology. 2012; 55:2005–2023. [PubMed: 22488764]
3. Krishnan B, Babu S, Walker J, Walker AB, Pappachan JM. Gastrointestinal complications of diabetes mellitus. World journal of diabetes. 2013; 4:51–63. [PubMed: 23772273]
4. Michelotti GA, Machado MV, Diehl AM. NAFLD, NASH and liver cancer. Nature reviews. Gastroenterology & hepatology. 2013; 10:656–665. [PubMed: 24080776]
5. Komander D, Rape M. The ubiquitin code. Annual review of biochemistry. 2012; 81:203–229.
6. Glickman MH, Ciechanover A. The ubiquitin-proteasome proteolytic pathway: destruction for the sake of construction. Physiological reviews. 2002; 82:373–428. [PubMed: 11917093]
7. Li W, et al. Genome-wide and functional annotation of human E3 ubiquitin ligases identifies MULAN, a mitochondrial E3 that regulates the organelle's dynamics and signaling. PloS one. 2008; 3:e1487. [PubMed: 18213395]
8. Semple CA, Group RG, Members GSL. The comparative proteomics of ubiquitination in mouse. Genome research. 2003; 13:1389–1394. [PubMed: 12819137]
9. Nakayama KI, Nakayama K. Ubiquitin ligases: cell-cycle control and cancer. Nature reviews. Cancer. 2006; 6:369–381. [PubMed: 16633365]
10. Skaar JR, Pagan JK, Pagano M. Mechanisms and function of substrate recruitment by F-box proteins. Nature reviews. Molecular cell biology. 2013; 14:369–381. [PubMed: 23657496]
11. Wang Z, Liu P, Inuzuka H, Wei W. Roles of F-box proteins in cancer. Nature reviews. Cancer. 2014; 14:233–247. [PubMed: 24658274]
12. Duda DM, et al. Structural regulation of cullin-RING ubiquitin ligase complexes. Current opinion in structural biology. 2011; 21:257–264. [PubMed: 21288713]
13. Jin J, et al. Systematic analysis and nomenclature of mammalian F-box proteins. Genes & development. 2004; 18:2573–2580. [PubMed: 15520277]
14. Bai C, et al. SKP1 connects cell cycle regulators to the ubiquitin proteolysis machinery through a novel motif, the F-box. Cell. 1996; 86:263–274. [PubMed: 8706131]
15. Frescas D, Pagano M. Deregulated proteolysis by the F-box proteins SKP2 and beta-TrCP: tipping the scales of cancer. Nature reviews. Cancer. 2008; 8:438–449. [PubMed: 18500245]
16. Kanarek N, Ben-Neriah Y. Regulation of NF-kappaB by ubiquitination and degradation of the IkappaBs. Immunological reviews. 2012; 246:77–94. [PubMed: 22435548]

17. Margottin-Goguet F, et al. Prophase destruction of Emi1 by the SCF(betaTrCP/Slimb) ubiquitin ligase activates the anaphase promoting complex to allow progression beyond prometaphase. Developmental cell. 2003; 4:813–826. [PubMed: 12791267]
18. Busino L, et al. Degradation of Cdc25A by beta-TrCP during S phase and in response to DNA damage. Nature. 2003; 426:87–91. [PubMed: 14603323]
19. Jin J, et al. SCFbeta-TRCP links Chk1 signaling to degradation of the Cdc25A protein phosphatase. Genes & development. 2003; 17:3062–3074. [PubMed: 14681206]
20. Shaik S, et al. SCF(beta-TRCP) suppresses angiogenesis and thyroid cancer cell migration by promoting ubiquitination and destruction of VEGF receptor 2. The Journal of experimental medicine. 2012; 209:1289–1307. [PubMed: 22711876]
21. Gao D, et al. mTOR drives its own activation via SCF(betaTrCP)-dependent degradation of the mTOR inhibitor DEPTOR. Molecular cell. 2011; 44:290–303. [PubMed: 22017875]
22. Wang Z, et al. SCF(beta-TRCP) promotes cell growth by targeting PR-Set7/Set8 for degradation. Nature communications. 2015; 6:10185.
23. Winston JT, et al. The SCFbeta-TRCP-ubiquitin ligase complex associates specifically with phosphorylated destruction motifs in IkappaBalpha and beta-catenin and stimulates IkappaBalpha ubiquitination in vitro. Genes & development. 1999; 13:270–283. [PubMed: 9990852]
24. Reue K, Zhang P. The lipin protein family: dual roles in lipid biosynthesis and gene expression. FEBS letters. 2008; 582:90–96. [PubMed: 18023282]
25. Peterfy M, Phan J, Xu P, Reue K. Lipodystrophy in the fld mouse results from mutation of a new gene encoding a nuclear protein, lipin. Nature genetics. 2001; 27:121–124. [PubMed: 11138012]
26. Reue K, Xu P, Wang XP, Slavin BG. Adipose tissue deficiency, glucose intolerance, and increased atherosclerosis result from mutation in the mouse fatty liver dystrophy (fld) gene. Journal of lipid research. 2000; 41:1067–1076. [PubMed: 10884287]
27. Langner CA, et al. The fatty liver dystrophy (fld) mutation. A new mutant mouse with a developmental abnormality in triglyceride metabolism and associated tissue-specific defects in lipoprotein lipase and hepatic lipase activities. The Journal of biological chemistry. 1989; 264:7994–8003. [PubMed: 2722772]
28. Han GS, Wu WI, Carman GM. The Saccharomyces cerevisiae Lipin homolog is a Mg2+-dependent phosphatidate phosphatase enzyme. The Journal of biological chemistry. 2006; 281:9210–9218. [PubMed: 16467296]
29. Finck BN, et al. Lipin 1 is an inducible amplifier of the hepatic PGC-1alpha/PPARalpha regulatory pathway. Cell metabolism. 2006; 4:199–210. [PubMed: 16950137]
30. Donkor J, Sariahmetoglu M, Dewald J, Brindley DN, Reue K. Three mammalian lipins act as phosphatidate phosphatases with distinct tissue expression patterns. The Journal of biological chemistry. 2007; 282:3450–3457. [PubMed: 17158099]
31. Santos-Rosa H, Leung J, Grimsey N, Peak-Chew S, Siniossoglou S. The yeast lipin Smp2 couples phospholipid biosynthesis to nuclear membrane growth. The EMBO journal. 2005; 24:1931–1941. [PubMed: 15889145]
32. Chen Z, Gropler MC, Mitra MS, Finck BN. Complex interplay between the lipin 1 and the hepatocyte nuclear factor 4 alpha (HNF4alpha) pathways to regulate liver lipid metabolism. PloS one. 2012; 7:e51320. [PubMed: 23236470]
33. Manmontri B, et al. Glucocorticoids and cyclic AMP selectively increase hepatic lipin-1 expression, and insulin acts antagonistically. Journal of lipid research. 2008; 49:1056–1067. [PubMed: 18245816]
34. Peterson TR, et al. mTOR complex 1 regulates lipin 1 localization to control the SREBP pathway. Cell. 2011; 146:408–420. [PubMed: 21816276]
35. Horton JD, Goldstein JL, Brown MS. SREBPs: activators of the complete program of cholesterol and fatty acid synthesis in the liver. The Journal of clinical investigation. 2002; 109:1125–1131. [PubMed: 11994399]
36. Inuzuka H, et al. Phosphorylation by casein kinase I promotes the turnover of the Mdm2 oncoprotein via the SCF(beta-TRCP) ubiquitin ligase. Cancer cell. 2010; 18:147–159. [PubMed: 20708156]

37. Orian A, et al. SCF(beta)(-TrCP) ubiquitin ligase-mediated processing of NF-kappaB p105 requires phosphorylation of its C-terminus by IkappaB kinase. The EMBO journal. 2000; 19:2580–2591. [PubMed: 10835356]
38. Chen H, et al. DNA damage regulates UHRF1 stability via the SCF(beta-TrCP) E3 ligase. Molecular and cellular biology. 2013; 33:1139–1148. [PubMed: 23297342]
39. Zhong J, et al. SCF beta-TRCP targets MTSS1 for ubiquitination-mediated destruction to regulate cancer cell proliferation and migration. Oncotarget. 2013; 4:2339–2353. [PubMed: 24318128]
40. Wu G, et al. Structure of a beta-TrCP1-Skp1-beta-catenin complex: destruction motif binding and lysine specificity of the SCF(beta-TrCP1) ubiquitin ligase. Molecular cell. 2003; 11:1445–1456. [PubMed: 12820959]
41. Reue K. The lipin family: mutations and metabolism. Current opinion in lipidology. 2009; 20:165–170. [PubMed: 19369868]
42. Liu GH, Gerace L. Sumoylation regulates nuclear localization of lipin-1alpha in neuronal cells. PloS one. 2009; 4:e7031. [PubMed: 19753306]
43. Wei H, et al. Sumoylation delimits KLF8 transcriptional activity associated with the cell cycle regulation. The Journal of biological chemistry. 2006; 281:16664–16671. [PubMed: 16617055]
44. Rena G, Bain J, Elliott M, Cohen P. D4476, a cell-permeant inhibitor of CK1, suppresses the site-specific phosphorylation and nuclear exclusion of FOXO1a. EMBO reports. 2004; 5:60–65. [PubMed: 14710188]
45. Breitkopf SB, Yuan M, Helenius KP, Lyssiotis CA, Asara JM. Triomics Analysis of Imatinib-Treated Myeloma Cells Connects Kinase Inhibition to RNA Processing and Decreased Lipid Biosynthesis. Analytical chemistry. 2015; 87:10995–11006. [PubMed: 26434776]
46. Duvel K, et al. Activation of a metabolic gene regulatory network downstream of mTOR complex 1. Molecular cell. 2010; 39:171–183. [PubMed: 20670887]
47. Porstmann T, et al. SREBP activity is regulated by mTORC1 and contributes to Akt-dependent cell growth. Cell metabolism. 2008; 8:224–236. [PubMed: 18762023]
48. Han J, et al. The CREB coactivator CRTC2 controls hepatic lipid metabolism by regulating SREBP1. Nature. 2015; 524:243–246. [PubMed: 26147081]
49. Zhao Y, Xiong X, Sun Y. DEPTOR, an mTOR inhibitor, is a physiological substrate of SCF(betaTrCP) E3 ubiquitin ligase and regulates survival and autophagy. Molecular cell. 2011; 44:304–316. [PubMed: 22017876]
50. Duan S, et al. mTOR generates an auto-amplification loop by triggering the betaTrCP- and CK1alpha-dependent degradation of DEPTOR. Molecular cell. 2011; 44:317–324. [PubMed: 22017877]
51. Nakayama K, et al. Impaired degradation of inhibitory subunit of NF-kappa B (I kappa B) and beta-catenin as a result of targeted disruption of the beta-TrCP1 gene. Proceedings of the National Academy of Sciences of the United States of America. 2003; 100:8752–8757. [PubMed: 12843402]
52. Dorrello NV, et al. S6K1- and betaTRCP-mediated degradation of PDCD4 promotes protein translation and cell growth. Science. 2006; 314:467–471. [PubMed: 17053147]
53. Peschiaroli A, et al. SCFbetaTrCP-mediated degradation of Claspin regulates recovery from the DNA replication checkpoint response. Molecular cell. 2006; 23:319–329. [PubMed: 16885022]
54. Kim TY, et al. Substrate trapping proteomics reveals targets of the betaTrCP2/FBXW11 Ubiquitin ligase. Molecular and cellular biology. 2015; 35:167–181. [PubMed: 25332235]
55. Guardavaccaro D, et al. Control of chromosome stability by the beta-TrCP-REST-Mad2 axis. Nature. 2008; 452:365–369. [PubMed: 18354482]
56. Low TY, et al. A systems-wide screen identifies substrates of the SCFbetaTrCP ubiquitin ligase. Science signaling. 2014; 7:rs8. [PubMed: 25515538]
57. Li S, Chen XW, Yu L, Saltiel AR, Lin JD. Circadian metabolic regulation through crosstalk between casein kinase 1delta and transcriptional coactivator PGC-1alpha. Molecular endocrinology. 2011; 25:2084–2093. [PubMed: 22052997]
58. Brookheart RT, Lee CY, Espenshade PJ. Casein kinase 1 regulates sterol regulatory element-binding protein (SREBP) to control sterol homeostasis. The Journal of biological chemistry. 2014; 289:2725–2735. [PubMed: 24327658]

59. Kourti M, et al. CK1delta restrains lipin-1 induction, lipid droplet formation and cell proliferation under hypoxia by reducing HIF-1alpha/ARNT complex formation. Cellular signalling. 2015; 27:1129–1140. [PubMed: 25744540]

60. Takahashi JS, Hong HK, Ko CH, McDearmon EL. The genetics of mammalian circadian order and disorder: implications for physiology and disease. Nature reviews. Genetics. 2008; 9:764–775.

61. Harris TE, Finck BN. Dual function lipin proteins and glycerolipid metabolism. Trends in endocrinology and metabolism: TEM. 2011; 22:226–233. [PubMed: 21470873]

62. Koh YK, et al. Lipin1 is a key factor for the maturation and maintenance of adipocytes in the regulatory network with CCAAT/enhancer-binding protein alpha and peroxisome proliferator-activated receptor gamma 2. The Journal of biological chemistry. 2008; 283:34896–34906. [PubMed: 18930917]

63. Phan J, Peterfy M, Reue K. Lipin expression preceding peroxisome proliferator-activated receptor-gamma is critical for adipogenesis in vivo and in vitro. The Journal of biological chemistry. 2004; 279:29558–29564. [PubMed: 15123608]

64. Phan J, Reue K. Lipin, a lipodystrophy and obesity gene. Cell metabolism. 2005; 1:73–83. [PubMed: 16054046]

65. Inuzuka H, et al. Acetylation-dependent regulation of Skp2 function. Cell. 2012; 150:179–193. [PubMed: 22770219]

66. Liu P, et al. Cell-cycle-regulated activation of Akt kinase by phosphorylation at its carboxyl terminus. Nature. 2014; 508:541–545. [PubMed: 24670654]

67. Gao D, et al. Phosphorylation by Akt1 promotes cytoplasmic localization of Skp2 and impairs APCCdh1-mediated Skp2 destruction. Nature cell biology. 2009; 11:397–408. [PubMed: 19270695]

68. Liu P, et al. Akt-mediated phosphorylation of XLF impairs non-homologous end-joining DNA repair. Molecular cell. 2015; 57:648–661. [PubMed: 25661488]

69. Jin J, Ang XL, Shirogane T, Wade Harper J. Identification of substrates for F-box proteins. Methods in enzymology. 2005; 399:287–309. [PubMed: 16338364]

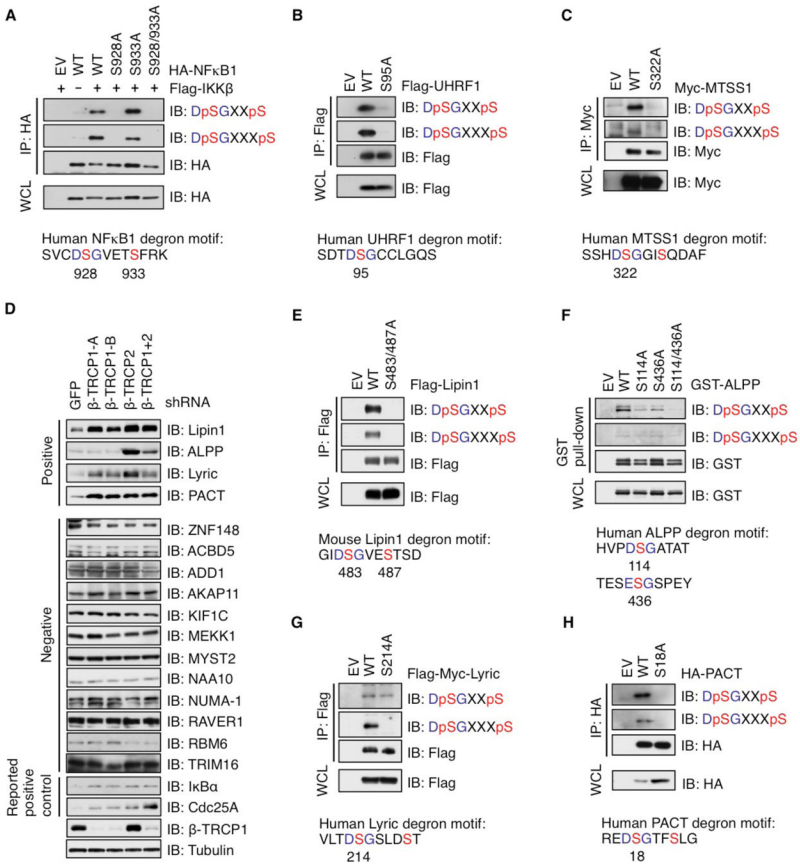

Fig. 1. Validation of anti-β-TRCP phospho-degron antibodies

(A) Immunoblot (IB) analysis of whole cell lysates (WCL) and immunoprecipitates (IP) derived from HeLa cells transfected with empty vector (EV), HA-NF-κB1 (p105) or Flag-IKKβ constructs as indicated and treated with MG132 before harvesting. N=2 biological replicates.

(B) IB analysis of WCL and IP derived from HeLa cells transfected with EV or the indicated Flag-UHRF1 constructs and treated with MG132 before harvesting. N=2 biological replicates.

(C)IB analysis of WCL and IP derived from HeLa cells transfected with EV or the indicated Myc-MTSS1 constructs and treated with MG132 before harvesting. N=2 biological replicates.

(D) HeLa cells were infected with shRNA lentiviral vectors specific for *GFP*, *β-TRCP1* (two independent shRNA constructs namely, -A, and -B), *β-TRCP2*, or *β-TRCP1+2* (shRNA against both *β-TRCP1* and *β-TRCP2* isoforms), subjected to puromycin selection and analyzed by IB. N=2 biological replicates.

(E) IB analysis of WCL and IP derived from HeLa cells transfected with EV or the indicated Flag-Lipin1 constructs and treated with MG132 before harvesting. N=2 biological replicates.

(F) IB analysis of WCL and IP derived from HeLa cells transfected with EV or the indicated GST-ALPP constructs and treated with MG132 before harvesting. N=2 biological replicates.

(G)IB analysis of WCL and IP derived from HeLa cells transfected with EV or the indicated Flag-Myc-tagged Lyric constructs and treated with MG132 before harvesting. N=2 biological replicates.

(H)IB analysis of WCL and IP derived from HeLa cells transfected with EV or the indicated HA-PACT constructs and treated with MG132 before harvesting. N=2 biological replicates.

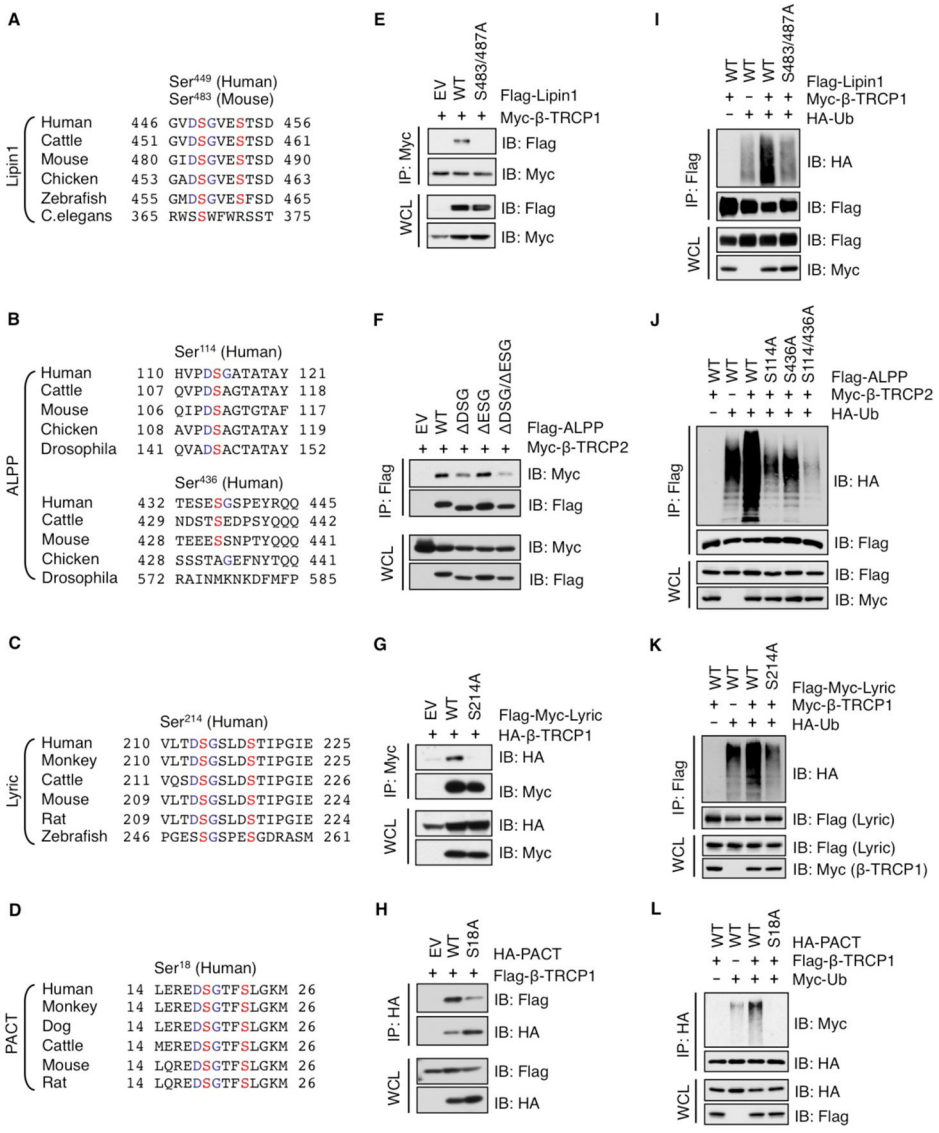

Fig. 2. Validation of Lipin1, ALPP, Lyric and PACT as SCF$^{\beta\text{-TRCP}}$ substrates

(A to **D)** Alignment of β-TRCP phospho-degron motifs in Lipin1 (A), ALPP (B), Lyric (C) and PACT (D) among different species.

(E) Immunoblot (IB) analysis of whole cell lysates (WCL) and immunoprecipitates (IP) derived from HeLa cells transfected with Myc-β-TRCP1 and empty vector (EV) or the indicated Flag-Lipin1 constructs and treated with MG132 before harvesting. N=2 biological replicates.

(F) IB analysis of WCL and IP derived from 293T cells transfected with Myc-β-TRCP2 and EV or the indicated Flag-ALPP constructs and treated with MG132 before harvesting. ΔDSG: DSG-motif-deletion, ΔESG: ESG-motif-deletion, ΔDSG/ΔESG: DSG/ESG-motif deletion. N=2 biological replicates.

(G) IB analysis of WCL and IP derived from 293T cells transfected with HA-β-TRCP1 and EV or the indicated Flag-Myc Lyric constructs and treated with MG132 before harvesting. N=2 biological replicates.

(H) IB analysis of WCL and IP derived from 293T cells transfected with Flag-β-TRCP1 and EV or HA-PACT constructs and treated with MG132 before harvesting. N=2 biological replicates.

(I) IB analysis of WCL and IP derived from 293T cells transfected with HA-tagged ubiquitin (HA-Ub), Myc-β-TRCP1 and Flag-mouse Lipin1 constructs as indicated and treated with MG132 before harvesting. N=2 biological replicates.

(J) IB analysis of WCL and IP derived from 293T cells transfected with HA-Ub, Myc-β-TRCP2 and Flag-ALPP constructs as indicated and treated with MG132 before harvesting. N=2 biological replicates.

(K) IB analysis of WCL and IP derived from 293T cells transfected with HA-Ub, Myc-β-TRCP1 and Flag-Myc-Lyric constructs as indicated and treated with MG132 before harvesting. N=2 biological replicates.

(L) IB analysis of WCL and IP derived from 293T cells transfected with Myc-Ub, Flag-β-TRCP1 and HA-PACT constructs as indicated and treated with MG132 before harvesting. N=2 biological replicates.

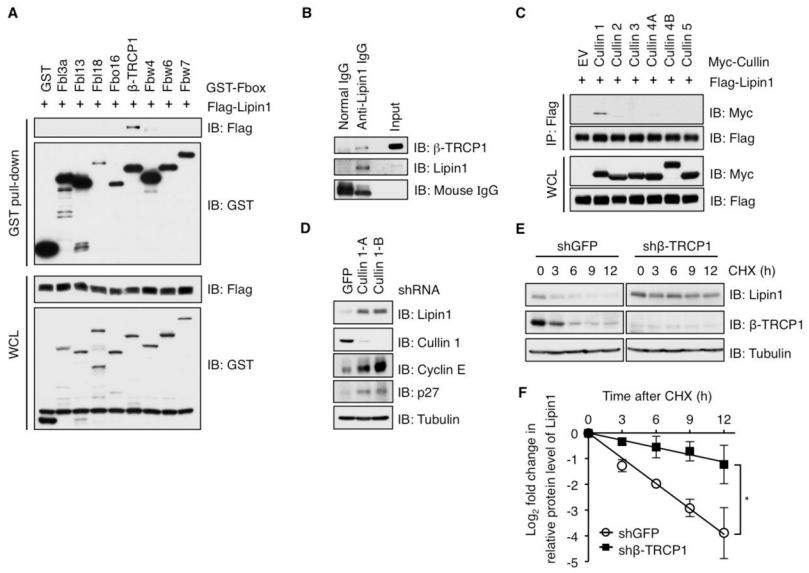

Fig. 3. SCF$^{\beta\text{-TRCP}}$ E3 ligase complex associates with Lipin1 to control its stability

(A) Immunoblot (IB) analysis of whole cell lysates (WCL) and GST pull-downs derived from 293T cells transfected with Flag-Lipin1 and the indicated GST-F-box protein constructs. N=2 biological replicates.

(B) IB analysis of WCL and anti-Lipin1 antibody-immunopreciptates (IP) derived from MDA-MB-231 cells. Normal mouse IgG was used for control IP. N=2 biological replicates.

(C)IB analysis of WCL and IP derived from 293T cells transfected with Flag-Lipin1 and empty vector (EV) or the indicated Myc-Cullin isoforms and treated with MG132 before harvesting. N=2 biological replicates.

(D) HeLa cells were infected with shRNA (sh) lentiviral vectors against *GFP* or *Cullin 1* (two independent shRNAs, namely, -A and -B), subjected to puromycin selection, and analyzed by IB. N=2 biological replicates.

(E) HeLa cells stably expressing shRNA against *GFP* or *β-TRCP1* were treated with cycloheximide (CHX) for the indicated times before harvesting. N=3 independent experiments.

(F) Quantification of the band intensities of (E). Lipin1 band intensities were normalized to the t = 0 time point. Data are presented as mean ± SD (N=3 independent experiments), * $p < 0.05$.

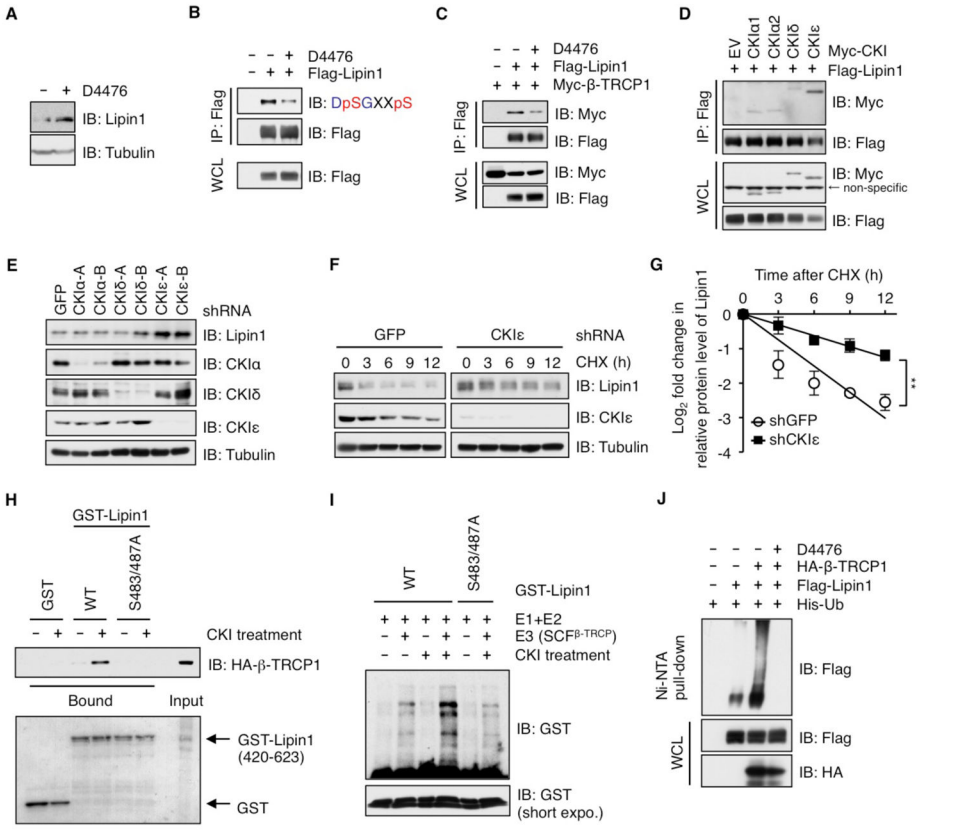

Fig. 4. Casein Kinase I (CKI) phosphorylates β-TRCP degron in Lipin1 to promote SCF$^{β\text{-}TRCP}$-mediated ubiquitination and degradation of Lipin1

(A) Immunoblot (IB) analysis of whole cell lysates (WCL) derived from 293T cells treated with the CKI inhibitor D4476. N=2 biological replicates.

(B) IB analysis of WCL and immunoprecipitates (IP) derived from HeLa cells transfected with Flag-Lipin1 and treated with D4476 and MG132 before harvesting. N=2 biological replicates.

(C)IB analysis of WCL and IP derived from 293T cells transfected with Myc-β-TRCP1 and empty vector (EV) or Flag-Lipin1 as indicated and treated with D4476 and MG132 before harvesting. N=2 biological replicates.

(D)IB analysis of WCL and IP derived from 293T cells transfected with Flag-Lipin1 and EV or Myc-CKI isoforms and treated with MG132 before harvesting. N=2 biological replicates.

(E) IB analysis of WCL derived from HeLa cells infected with lentiviral shRNA vectors against *GFP*, *CKIα* (two independent shRNAs, -A and -B), *CKIδ* (two independent shRNAs, -A and -B), or *CKIε* (two independent shRNAs, -A and -B), subjected to puromycin selection, and analyzed by IB. N=2 biological replicates.

(F) HeLa cells stably expressing shRNA against *GFP* or *CKIε* were treated with cycloheximide (CHX) for the indicated times before harvesting and IB analysis. N=3 independent experiments.

(G) Quantification of the band intensities in (F). Data are presented as mean ± SD (N=3 independent experiments), ** $p < 0.01$.

(H)IB analysis showing the recovery of HA-β-TRCP1 bound to the GST-Lipin1 (420–623) recombinant proteins (or GST as a negative control) with or without treatment with recombinant CKI. Ponceau S staining (bottom panel) was performed to indicate equal loading of the indicated GST-fusion proteins. N=2 biological replicates.

(I) IB analysis indicating that $SCF^{\beta\text{-}TRCP1}$ E3 ligase complex promotes Lipin1 polyubiquitination in a CKI-dependent manner. Where indicated, recombinant GST-Lipin1 (420–623) proteins were pretreated with recombinant CKI before the in vitro ubiquitination assays. N=2 biological replicates.

(J) 293T cells were transfected with His-tagged ubiquitin (His-Ub), Flag-Lipin1 and HA-β-TRCP1 as indicated and treated with MG132 in the absence or presence of D4476. Ubiquitin-conjugated proteins were captured with Ni-NTA-agarose beads and subjected to IB analysis. Ni-NTA: Ni(2+)-nitrilotriacetic acid. N=2 biological replicates.

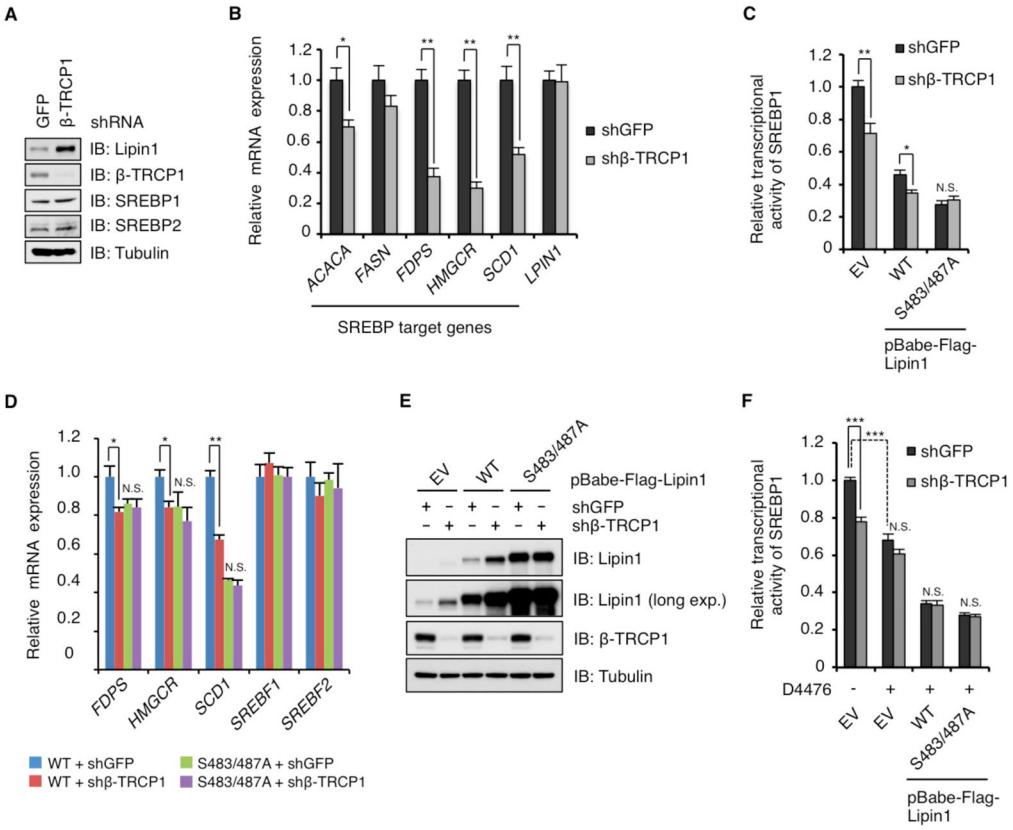

Fig. 5. β-TRCP promotes SREBP-dependent transcriptional activities by targeting Lipin1 for degradation

(A) Immunoblot (IB) analysis of whole cell lysate (WCL) derived from NIH-3T3 cells infected with lentiviral shRNA vectors against *GFP* or *β-TRCP1* and subjected to puromycin selection before harvesting. N=2 biological replicates.

(B) Real-time RT-PCR analysis to examine the relative mRNA expression of various SREBP target genes in NIH3T3 cells generated in (A). *36B4* was utilized for normalization. Data are presented as mean ± SEM, N=3 biological replicates. * $p < 0.05$, ** $p < 0.01$.

(C)NIH-3T3 cells were infected with the retroviral pBabe-Flag-Lipin1 expression vector and the indicated lentiviral shRNA construct and subjected to hygromycin/puromycin selection (these cells were also used in Fig. 5, D to F). Cells were then transfected with the SREBP1-luciferase reporter and HA-SREBP1 expression plasmids. Relative SREBP1 transcriptional activity was measured in cell lysates. Data are presented as mean ± SD, N=4 biological replicates, * $p < 0.05$, ** $p < 0.01$. N.S., not significant.

(D) Real-time RT-PCR analysis to examine the relative mRNA expression of SREBP target genes in NIH-3T3 cells generated in (C). *36B4* was utilized for normalization. Data are presented as mean ± SEM, N=3 biological replicates, * $p < 0.05$, ** $p < 0.01$. N.S., not significant.

(E) IB analysis of WCL derived from NIH-3T3 cells generated in (C). N=2 biological replicates.

(F) Relative SREBP1 transcriptional activity was measured in NIH-3T3 cells generated in (C), which were transfected with SREBP1-luciferase reporter plasmid and HA-SREBP1.

Cells were treated with D4476 before harvesting. Data are presented as mean ± SD, N=6 biological replicates, *** $p < 0.001$. N.S., not significant.

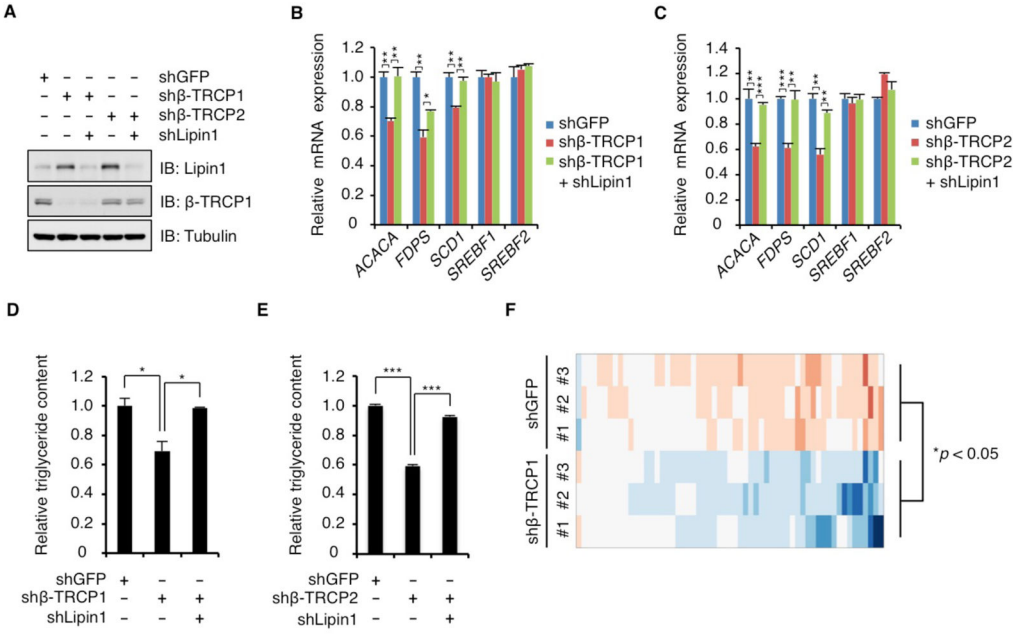

Fig. 6. β-TRCP controls lipogenesis in a Lipin1 dependent manner in hepatocyte

(A) Immunoblot (IB) analysis of HepG2 cells infected with lentiviral shRNA (sh) vectors as indicated, which were subjected to puromycin selection before harvesting. N=2 biological replicates.

(B and **C)** Real-time RT-PCR analysis to examine the relative mRNA expression of SREBP target genes in HepG2 cells generated in (A). *36B4* was utilized for normalization. Data are presented as mean ± SEM, N=3 biological replicates. * $p < 0.05$, ** $p < 0.01$, *** $p < 0.001$.

(D and **E)** Relative triglyceride content was examined in HepG2 cells that were infected with the indicated lentiviral shRNA constructs and subjected to puromycin selection before harvesting. Data are presented as mean ± SEM, N=3 biological replicates, * $p < 0.05$, *** $p < 0.001$.

(F) Relative triglyceride content was examined by mass spectrometry-based lipidomics approach in HepG2 cells that were infected with the indicated lentiviral shRNA constructs and subjected to puromycin selection. Lipid ion peak area intensities represent the normalized (by cellular protein content), integrated MS1 total ion current are expressed as median-centered values across all samples. Differential amounts of triglyceride are indicated by color intensity of individual triglyceride species' column: red (up) and blue (down). N=3 biological replicates.

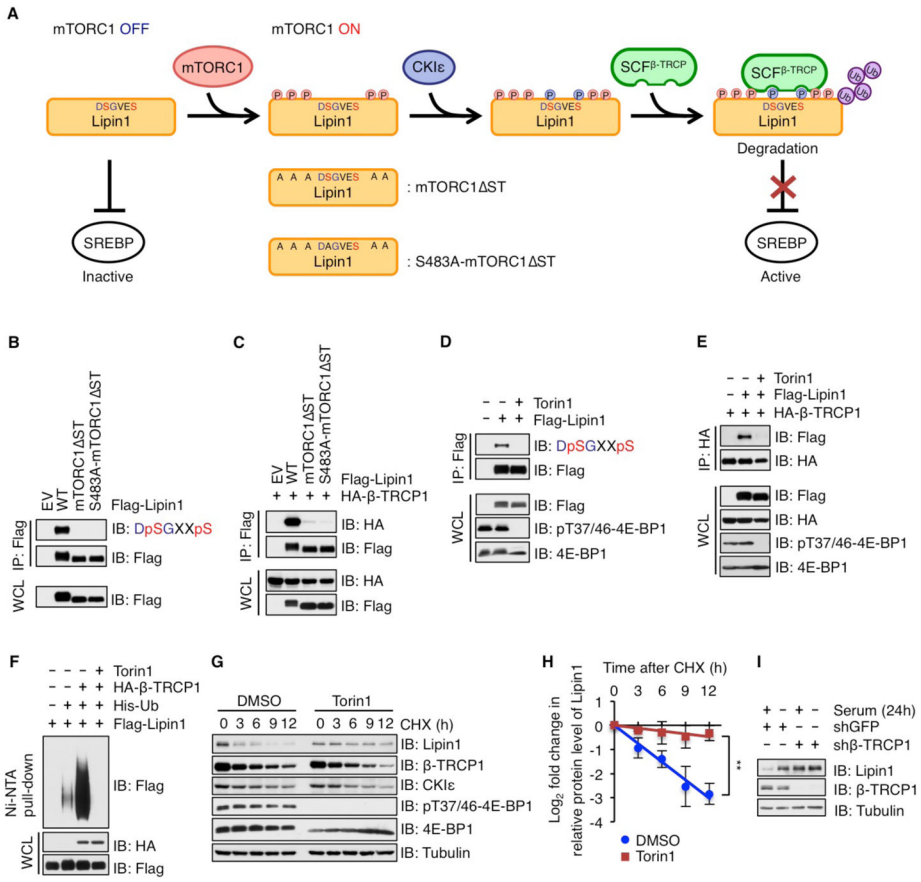

Fig. 7. mTORC1 functions as a priming kinase for CKI to promote β-TRCP-mediated Lipin1 degradation

(A) Schematic model to illustrate the regulation of Lipin1 abundance by the mTORC1/CKI/β-TRCP signaling axis, and schematic diagram of Lipin1 constructs used in Fig. 7, B and C.

(B) Immunoblot (IB) analysis of whole cell lysates (WCL) and immunoprecipitates (IP) derived from 293 cells transfected with empty vector (EV) or the indicated Flag-Lipin1 constructs and treated with MG132 before harvesting. N=2 biological replicates.

(C) IB analysis of WCL and IP derived from 293 cells transfected with HA-β-TRCP1 and EV or the indicated Flag-Lipin1 constructs and treated with MG132 before harvesting. N=2 biological replicates.

(D) IB analysis of WCL and IP derived from HeLa cells transfected with EV or Flag-Lipin1, and then treated with Torin1 and MG132 before harvesting. N=2 biological replicates.

(E) IB analysis of WCL and IP derived from HeLa cells transfected with HA-β-TRCP1 and EV or Flag-Lipin1 as indicated, and then treated with Torin1 and MG132 before harvesting. N=2 biological replicates.

(F) 293T cells were transfected with His-tagged ubiquitin (His-Ub), Flag-Lipin1 and HA-β-TRCP1 as indicated and treated with MG132 in the absence or presence of Torin1. Ubiquitin-conjugated proteins were captured with Ni-NTA-agarose beads and subjected to IB analysis. Ni-NTA: Ni(2+)-nitrilotriacetic acid. N=2 biological replicates.

(G) IB analysis of WCL derived from HepG2 cells. After pretreatment with Torin1, the cells were treated with cycloheximide (CHX) for the indicated time periods before harvesting. N=3 independent experiments.

(H) Quantification of the band intensities in (G). Data are presented as mean ± SD (N=3 independent experiments), ** $p < 0.01$.

(I) IB analysis of WCL derived from HepG2 cells infected with lentiviral shRNA vectors as indicated and subjected to puromycin selection. The resulting cell lines were deprived of serum before harvesting. N=2 biological replicates.

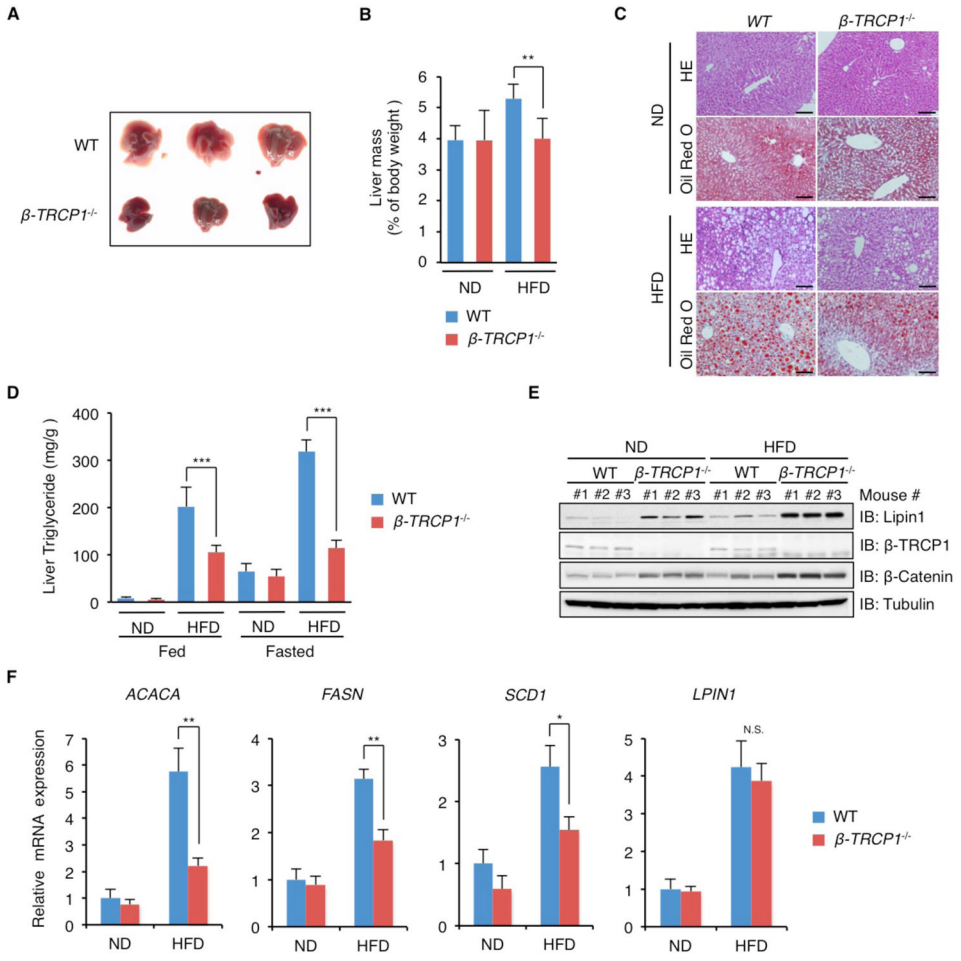

Fig. 8. *β-TRCP1*$^{-/-}$ mice are protected from high fat diet-induced hepatic steatosis

(A) Representative images of liver from wild-type (WT) and *β-TRCP1*$^{-/-}$ mice fed with high fat diet (HFD).

(B) Liver mass was measured from WT (n=5) and *β-TRCP1*$^{-/-}$ (n=5) mice fed with normal diet (ND) or HFD as indicated. Data are presented as mean ± SD, ** $p < 0.01$.

(C) Representative images of hematoxylin/eosin (HE)-stained section and Oil-Red O stained of liver from WT or *β-TRCP1*$^{-/-}$ mice fed with ND or HFD as indicated. Scale bar = 100 μm

(D) Liver triglyceride content normalized to liver weight was measured from WT (n=6) and *β-TRCP1*$^{-/-}$ (n=6) mice fed with ND or HFD in fed or fasted conditions as indicated. Data are presented as mean ± SD, *** $p < 0.001$.

(E) Immunoblot (IB) analysis of lysates derived from liver of WT and *β-TRCP1*$^{-/-}$ mice fed with ND or HFD. n=3 mice for each group.

(F) Real-time RT-PCR analysis of *ACACA, FASN, SCD1* and *LPIN1* mRNA in liver of WT (n=6) and *β-TRCP1*$^{-/-}$ (n=6) mice fed with ND or HFD as indicated. *36B4* was utilized for normalization. Data are presented as mean ± SD, * $p < 0.05$, ** $p < 0.01$. N.S., not significant.